HAL
open science

Coherent frequency conversion in a superconducting artificial atom with two internal degrees of freedom

Florent Lecocq, Ioan M. Pop, Iulian Matei, Etienne Dumur, A. K. Feofanov, Cécile Naud, Wiebke Guichard, Olivier Buisson

To cite this version:

Florent Lecocq, Ioan M. Pop, Iulian Matei, Etienne Dumur, A. K. Feofanov, et al.. Coherent frequency conversion in a superconducting artificial atom with two internal degrees of freedom. Physical Review Letters, 2012, 108 (10), pp.107001. 10.1103/PhysRevLett.108.107001 . hal-00661286

HAL Id: hal-00661286

https://hal.science/hal-00661286

Submitted on 19 Jan 2012

HAL is a multi-disciplinary open access archive for the deposit and dissemination of scientific research documents, whether they are published or not. The documents may come from teaching and research institutions in France or abroad, or from public or private research centers.

L'archive ouverte pluridisciplinaire **HAL**, est destinée au dépôt et à la diffusion de documents scientifiques de niveau recherche, publiés ou non, émanant des établissements d'enseignement et de recherche français ou étrangers, des laboratoires publics ou privés.

Coherent frequency conversion in a superconducting artificial atom with two internal degrees of freedom

F. Lecocq, I. M. Pop, I. Matei, E. Dumur, A. K. Feofanov, C. Naud, W. Guichard, O. Buisson
Institut Néel, C.N.R.S.- Université Joseph Fourier, BP 166, 38042 Grenoble-cedex 9, France
(Dated: January 19, 2012)

By adding a large inductance in a dc-SQUID phase qubit loop, one decouples the junctions' dynamics and creates a superconducting artificial atom with two internal degrees of freedom. In addition to the usual symmetric plasma mode (s-mode) which gives rise to the phase qubit, an anti-symmetric mode (a-mode) appears. These two modes can be described by two anharmonic oscillators with eigenstates $|n_s\rangle$ and $|n_a\rangle$ for the s and a-mode, respectively. We show that a strong nonlinear coupling between the modes leads to a large energy splitting between states $|0_s, 1_a\rangle$ and $|2_s, 0_a\rangle$. Finally, coherent frequency conversion is observed via free oscillations between the states $|0_s, 1_a\rangle$ and $|2_s, 0_a\rangle$.

PACS numbers:

In atomic physics the presence of multiple degrees of freedom (DoF) constitutes a precious resource for the development of quantum mechanics experiments. In trapped ions or nitrogen-vacancy centers, the V-shaped energy spectrum enables very high fidelity readout of the states encoded in the first two levels by using the fluorescence properties of the transition to the third level [1, 2]. In quantum optics, the multiple DoF of the optically active crystals have lead to many quantum effects such as Coherent Population Trapping (CPT) and the associated effect of Electromagnetically Induced Transparency (EIT) [3], spontaneous emission cancelation via quantum interference [4, 5] or generation of entangled photon pairs [6]. In the field of superconducting qubits, experimental efforts have mainly focused on two-level systems [7, 8] and multilevel systems [9–13] with a single DoF. Superconducting artificial atoms currently need additionnal DoF in order to realize Λ, V, N or diamond-shaped energy levels and therefore to perform new quantum experiments [14, 15]. Only recently a superconducting device with V-shape energy spectrum was experimentally considered [16] and a three DoF superconducting ring was developed for parametric amplification [17].

In this letter we present an artificial atom with two internal DoF which constitutes a basic block for the realization of V- or Diamond-shaped energy levels. In this system we benefit from the natural nonlinear coupling between the two DoF to observe a coherent frequency conversion process in the time domain. Contrary to previous frequency conversion proposals and implementations in solid state devices, we observe this process in the strong coupling limit, where multiples oscillations can be seen before losing coherence [18, 19], and without any external coupling device or additionnal source of power [20]. In addition this system could be used for triggered and high-efficiency generation of entangled pairs of photons, a key component for quantum information [21].

The circuit is a camelback phase qubit [22] with a large loop inductance, *i.e* a dc-SQUID build by a superconducting loop of large inductance L interrupted by two identical Josephson junctions with critical current I_c and capacitance C, operated at zero current bias (see Fig.1). As we will see in the following, the presence of a large loop inductance modifies dractically the quantum dynamics of this system. The two phase differences ϕ_1 and ϕ_2 across the two junctions correspond to the two degrees of freedom of this circuit, which lead to two oscillating modes: the symmetric (s-) and the anti-symmetric (a-) plasma modes [23]. The s-mode corresponds to the well-known in-phase plasma oscillation of the two junctions with the average phase $x_s = (\phi_1 + \phi_2)/2$, oscillating at a characteristic frequency given by the plasma frequency of the dc-SQUID, ω_p^s. The a-mode is an opposite-phase plasma mode related to oscillations of the phase difference $x_a = (\phi_1 - \phi_2)/2$, producing circulating current oscillations at frequency ω_p^a. In previous experiments [9, 11, 22] , the loop inductance L was small compared to the Josephson inductance $L_J = \Phi_0/(2\pi I_c)$. Therefore the two junctions were strongly coupled and the dynamics of the phase difference x_a was neglected and fixed by the applied flux. The quantum behavior of the circuit was described by the s-mode only, showing a one-dimensional motion of the average phase x_s. Hereafter we will consider a circuit with a large inductance ($L \geq L_J$) that decouples the phase dynamics of the two junctions. This large inductance lowers the frequency of the a-mode and the dynamics of the system becomes fully two-dimensional. The a-mode was previously introduced to discuss the thermal and quantum escape of a current-biased dc-SQUID [24, 25] but its dynamics was never observed. We present measurements of the full spectrum of this artificial atom, independent coherent control of both modes and finally we exploit the strong nonlinear coupling between the two DoF to observe a time resolved up and down frequency conversion of the system excitations.

The electronic properties of a symmetric and inductive dc-SQUID at zero-current bias can be described by a fictitious particle of mass $m = 2C(\Phi_0/2\pi)^2$ moving inside

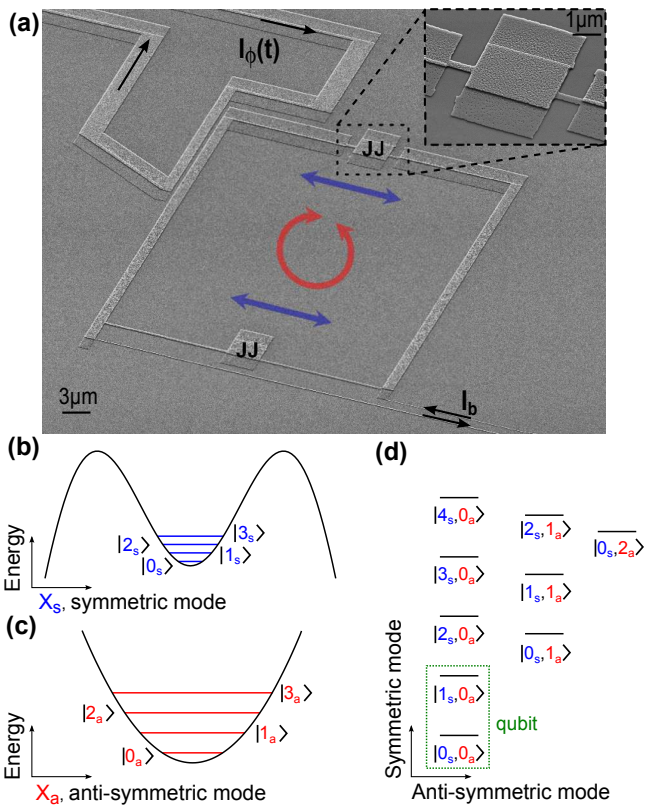

FIG. 1: **Description of the device**. **(a)** A micrograph of the aluminium circuit. The two small squares are the two Josephson junctions (enlarged in the top right inset, $10\mu m^2$ area, $I_c = 713$ nA and $C = 510$ fF) decoupled by a large inductive loop ($L = 629$ pH). The width of the two SQUID arms were adjusted to reduce the inductance asymmetry to about 10%. Very narrow current bias lines, with a large 15 nH-inductance, isolate the quantum circuit from the dissipative environment at high frequencies . The symmetric and anti-symmetric oscillation modes are illustrated by blue and red arrows, respectively. **(b)** and **(c)** Potentials of the s and a-mode respectively, for the bias working point ($I_b = 0$,$\Phi_b = 0.37\Phi_0$). **(d)** Schematic energy level diagram indexed by the quantum excitation number of the two modes $|n_s, n_a\rangle$ at the same working point. Climbing each vertical ladder one increases the excitation number of the s-mode, keeping the excitation number of the a-mode constant. The two first levels, $|0_s, 0_a\rangle$ and $|1_s, 0_a\rangle$, realize a camelback phase qubit.

a two-dimensional potential :

$$U(x_s, x_a) = 2E_J\left[-cosx_s cosx_a + \frac{L_J}{L}(x_a - \frac{\pi\Phi_b}{\Phi_0})^2\right] \quad (1)$$

where $E_J = \Phi_0 I_c/(2\pi)$. Hereafter we will consider the particle trapped in a local minimum (x_s^{min}, x_a^{min}) verifying $x_s^{min} = 0$ and $x_a^{min} + (L/2L_J)\sin x_a^{min} = \pi\Phi_b/\Phi_0$. By expanding the potential at this minimum up to fourth order, its quantum dynamics is given by the Hamiltonian $\mathcal{H} = \mathcal{H}_s + \mathcal{H}_a + \mathcal{C}_{s,a}$ where $\mathcal{H}_s$ and $\mathcal{H}_a$ are anharmonic oscillator Hamiltonians describing respectively the symmetric and antisymmetric plasma modes [26, 27]. $\mathcal{C}_{s,a}$ describes the coupling between the two oscillators. $\mathcal{H}_\alpha = \hbar\omega_p^\alpha\left[(\hat{p}_\alpha^2 + \hat{x}_\alpha^2)/2 - \sigma_\alpha\hat{x}_\alpha^3 + \delta_\alpha\hat{x}_\alpha^4\right]$, where $\alpha = s, a$ with $(\omega_p^s)^2 = (2E_J/m)\cos x_a^{min}$ and $(\omega_p^a)^2 = (\omega_p^s)^2 + (4E_J/m)(L_J/L)$. The operators $\hat{x}_\alpha$ and $\hat{p}_\alpha$ are the reduced position and momentum operators in both directions. The coupling term has a very simple expression at zero current bias:

$$\mathcal{C}_{s,a} = \hbar g_{21}\hat{x}_s^2\hat{x}_a + \hbar g_{22}\hat{x}_s^2\hat{x}_a^2 \quad (2)$$

with $\hbar g_{21} = -E_J(\hbar/m)^{\frac{3}{2}}(\omega_p^s\sqrt{\omega_p^a})^{-1}\sin x_a^{min}$ and $\hbar g_{22} = -E_J(\hbar/m)^2(\omega_p^s\omega_p^a)^{-1}\cos x_a^{min}/2$. In the following, we will define $|n_s, n_a\rangle \equiv |n_s\rangle|n_a\rangle$ as the eigenstates of uncoupled hamiltonian $\mathcal{H}_s + \mathcal{H}_a$, where $|n_\alpha\rangle$ indexes the energy levels of each mode. The potentials associated with the s-mode and a-mode are depicted in the figure Fig.1b and Fig.1c for a working point ($I_b = 0$, $\Phi_b = 0.37\Phi_0$). At the same bias point the complete spectrum of the system is presented in Fig.1d.

The complete aluminum device is fabricated using an angle evaporation technique without suspended bridges [28], and it is presented in Fig.1a. The measurements were conducted in a dilution refrigerator at 40 mK using a standard experimental configuration, previously described in Ref.[22].

The readout of the circuit is performed using switching current techniques. For spectroscopy measurements we apply a microwave pulse field, through the current bias line (see Fig 1a), followed by the readout nanosecond flux pulse that produces a selective escape depending on the quantum state of the circuit [9, 22]. The energy spectrum versus current bias at $\Phi_b = 0.48\Phi_0$ and versus flux bias at $I_b = 0$ are plotted in Fig.2a and Fig.2b respectively. In the following we will denote ν_{nm}^α as the transition frequency between the states $|n_\alpha\rangle$ and $|m_\alpha\rangle$, with the other mode in the ground state. The first transition frequency in Fig.2 is the one of the camelback phase qubit, ν_{01}^s. With a maximum frequency at zero-current bias, the system is at an optimal working point with respect to current fluctuations [22]. At higher frequency, the second transition of the s-mode is observed with $\nu_{02}^s \approx 2\nu_{01}^s$. In the flux biased spectrum the third transition ν_{03}^s is also visible. An additional transition is observed at about 14.6 GHz, with a very weak current dependence (Fig.2a) but a finite flux dependence (Fig.2b). It corresponds to the first transition of the a-mode, ν_{01}^a. The s-mode transition frequencies drop when Φ_b/Φ_0 approaches 0.7 which is consistent with the critical flux $\Phi_c/\Phi_0 = 1/2 + L/(2\pi L_J) = 0.717$ for which $\omega_p^s \to 0$ and $x_a^{min} \to \pi/2$. On the contrary ω_p^a remains finite when $\Phi_b \to \Phi_c$ with $\omega_p^a \to \sqrt{(4E_J/m)(L_J/L)}$. One also observes a large level anti-crossing of about 700 MHz between the two transitions ν_{02}^s and ν_{01}^a. Additionally no level anti-crossing is measurable between ν_{03}^s and ν_{01}^a.

The experimental energy spectrum in Fig.2 can be per-

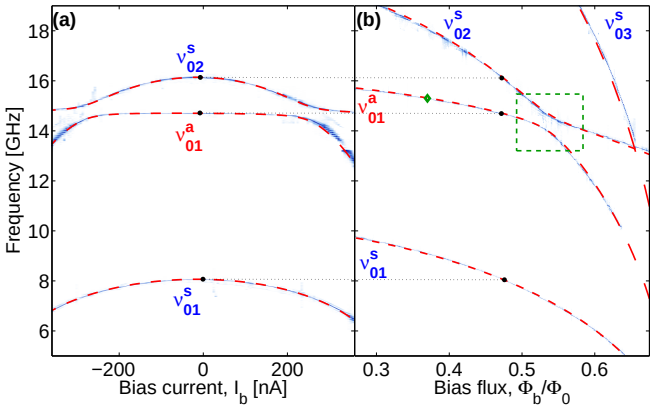

FIG. 2: **Energy spectrum**. Escape probability P_{esc} versus frequency as a function of current bias **(a)** and flux bias **(b)** measured at $\Phi_b = 0.48\Phi_0$ and $I_b = 0$ respectively. P_{esc} is enhanced when the frequency matches a resonant transition of the circuit. The microwave amplitude was tuned to keep the resonance peak amplitude at 10%. Dark and bright blue scale correspond to high and small P_{esc}. The red dashed lines are the transition frequencies deduced from the spectrum of the full hamiltonian with $C = 510$ fF (see text). The green diamond is the initial working point for the measurement of coherent free oscillations between the two modes, presented in Fig.3, and the green dotted square is the area where these oscillations take place.

fectly fitted by deriving the spectrum of the full Hamiltonian described above. As all the other parameters of the device can be extracted from switching-current measurements [22], the only free parameter is the junction capacitance. From the fit we obtain $C = 510$ fF, which is consistent with the $10\mu m^2$ junction area. Numerical calculations are used to describe the energy dependence in Fig.2a in order to take into account the current bias and the inductance asymmetry as well as additional coupling terms. The model describes well the level anti-crossing between the quantum states $|2_s, 0_a\rangle$ and $|0_s, 1_a\rangle$, which is given by the nonlinear coupling term $\hbar g_{21}\hat{x}_s^2\hat{x}_a$. The coupling strength $g_{21}/2\pi$ strongly depends on the working point. It is predicted to change from zero at $\Phi_b = 0$, to 700 MHz at the anti-crossing, up to about 1200 MHz at $\Phi_b \approx 0.65$ close to the critical line. The coupling term $\hat{x}_s^2\hat{x}_a$ mainly couples the states $|0_s, 1_a\rangle$ and $|2_s, 0_a\rangle$. Starting from these uncoupled states at $\Phi_b = 0$, they become a maximally entangled state at the resonance condition, $\nu_{01}^a = \nu_{02}^s$. Close to $\Phi_b = \Phi_c$ the states are still entangled because g_{21} diverges. In this device the second nonlinear coupling term, $\hat{x}_s^2\hat{x}_a^2$, is one order of magnitude smaller with $g_{22}/2\pi \approx 50$ MHz. Nevertheless the shift of transition frequencies that it induces must be taken into account to fit the experimental spectrum. Finally the absence of $\hat{x}_s^3\hat{x}_a$ in the coupling term explains why no level anti-crossing between ν_{03}^s and ν_{01}^a is observed.

From spectroscopic measurements, we obtain minimum resonance widths as narrow as 4 MHz and 3.5 MHz for the transitions ν_{01}^s and ν_{01}^a respectively. The corresponding dephasing times are estimated to be $T_2^s \approx 160$ ns and $T_2^a \approx 180$ ns. At the working point ($I_b = 0, \Phi_b = 0.37\Phi_0$) Rabi-like oscillations are performed on the s- and a-mode by applying microwave power at the resonance frequencies ν_{01}^s and ν_{01}^a respectively. Rabi-decay time is measured in the two-level limit with about 170 ns and 50 ns for s- and a-mode. Relaxation times $T_1^s = 200$ ns and $T_1^a = 74$ ns are extracted from the exponential population decay of the excited levels $|1_s, 0_a\rangle$ and $|0_s, 1_a\rangle$. The measured coherence times of the a-mode are much smaller than expected from the minimum linewidth. The origin of this additional decoherence will be discussed later. Nevertheless, the coherence time is sufficiently large for independent coherent control of each mode.

One of the opportunities given by the rich spectrum of this two DoF artificial atom is the observation of a coherent frequency conversion process using the $\hat{x}_s^2\hat{x}_a$ coupling of Eq.2. The pulse sequence, similar to other states swapping experiment [29, 30], is presented in (see Fig.3a). At $t = 0$, the system is prepared in the state $|0_s, 1_a\rangle$, at the initial working point $\Phi_b = 0.37\Phi_0$ (green diamond in Fig.2b). Immediately after, a non-adiabatic flux pulse [32] brings the system to the working point defined by Φ_{int}, close to the degeneracy point ($\nu_{02}^s \approx \nu_{01}^a$). After the free evolution of the quantum state during the time Δt_{int}, we measure the escape probility P_{esc}. Fig.3b presents P_{esc} as a function of Δt_{int} for $\Phi_{int} = 0.515\Phi_0$. The observed oscillations have a $815MHz$-characteristic frequency (inset of Fig.3b) that matches precisely the theoritical frequency splitting at this flux bias (red arrow). In Fig.3c, we present these oscillations as function of Φ_{int}. Their frequency varies with Φ_{int}, showing a typical "chevron" pattern. In the inset of Fig.3c, the oscillation frequency versus Φ_{int} is compared to theoretical predictions. The good agreement between theory and experiment is a striking confirmation of the observation of swapping between the quantum states $|0_s, 1_a\rangle$ and $|2_s, 0_a\rangle$. Instead of the well known linear coupling $\hat{x}_s\hat{x}_a$ between two oscillators, which corresponds to a coherent exchange of single excitations between the two systems, here the coupling $\hat{x}_s^2\hat{x}_a$ is non-linear and produces a coherent exchange of a single excitation of the a-mode with a double excitation of the s-mode, *i.e.* a coherent frequency conversion. Starting from the state $|0_s, 1_a\rangle$, an excitation pair $|2_s, 0_a\rangle$ is then deterministically produced in about a single nanosecond at the degeneracy point $\Phi_{int} = 0.537\Phi_0$.

We now discuss the coherent properties and measurement contrast in our device. The unexpectedly short coherence time of the a-mode can be explained by the coupling to spurious two-level systems (TLS) [31]. With a junction area of $10\mu m^2$ our device suffers from a large TLS density of about 12 TLS/GHz (barely visible in Fig.2). Therefore it is very difficult to operate the a-

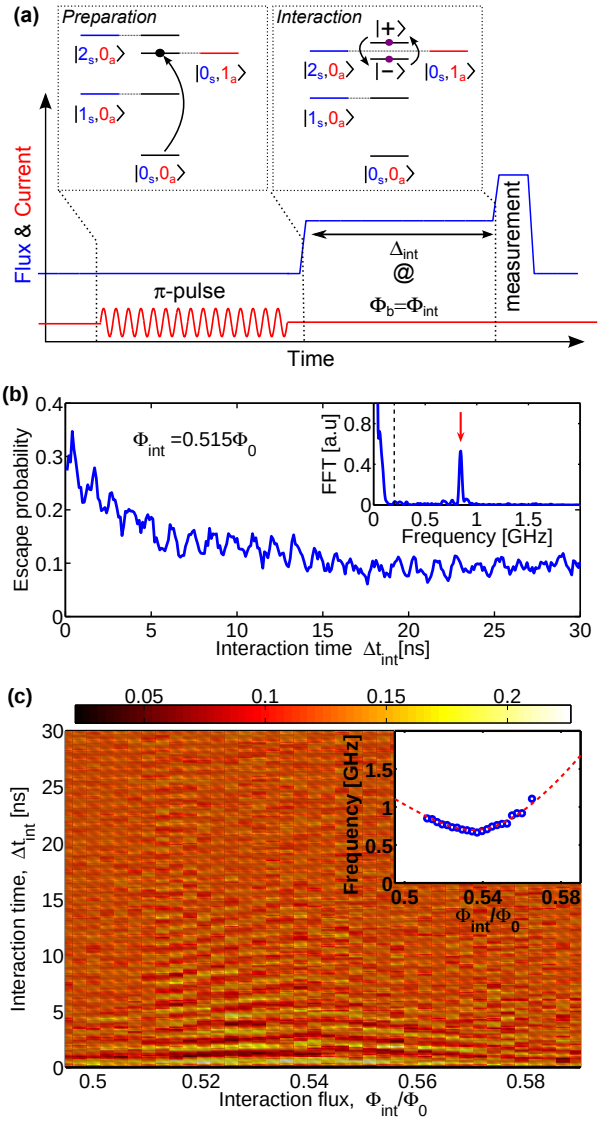

FIG. 3: **Free coherent oscillations between states $|0_s, 1_a\rangle$ and $|2_s, 0_a\rangle$ produced by a nonlinear coupling.** **(a)** Schematic pulse sequence. The energy diagram, without coupling in blue/red and with coupling in black, is represented for both the preparation and interaction steps.**(b)** Escape probability P_{esc} versus interaction time Δt_{int}. The inset presents the Fourier transform of these oscillations with a clear peak at 815 MHz. The red arrow indicates the theoretically expected frequency. **(c)** P_{esc} versus interaction time Δt_{int} for different interaction flux Φ_{int} close to the resonance condition between ν^s_{02} and ν^a_{01}. For clarity the data is numerically processed using 200 MHz high-pass filter(dashed line in inset of (b)). Inset : oscillation frequency as function of flux. The dashed red line shows the theoretical predictions.

mode in a frequency window free of TLS since ν^a_{01} is only slightly flux dependent. However this is not a real issue as it can be solved easily by reducing the junction area [33]. The minimum linewidth of both a-mode and s-mode, and therefore their coherence times, are limited in our experiment by low frequency flux noise. Operating the system at $\Phi_b = 0$ will lift this limitation since it is an optimal point with respect to flux noise. The small oscillation amplitude in Fig.3 has two additionnals origins. First the duration t_π of the π-pulse applied for preparation of the state $|0_s, 1_a\rangle$ has to fulfill the condition $t_\pi^{-1} < \nu^a_{12} - \nu^a_{01}$ to avoid multilevel dynamics. Since $\nu^a_{12} - \nu^a_{01} = 18$ MHz in the present experiment, we fixed $t_\pi = 80$ ns. However t_π is of the order the relaxation time of the a-mode which implies a strong reduction of the $|0_s, 1_a\rangle$ occupancy after the π-pulse, to about 40%. The second origin of the small contrast raises the question of the readout contrast between the states $|0_s, 1_a\rangle$ and $|2_s, 0_a\rangle$. In absence of coupling the escape probability of the state $|0_s, n_a\rangle$ should not be sensitive to n_a. On the contrary, the escape probability of the state $|n_s, 0_a\rangle$ is very sensitive to n_s. This difference should lead to a strong contrast between the states $|0_s, 1_a\rangle$ and $|2_s, 0_a\rangle$. However, since the coupling strength is very large close to the critical lines, $|0_s, 1_a\rangle$ and $|2_s, 0_a\rangle$ are still entangled when the escape occurs. This leads to an additionnal reduction of the contrast between the two states that prevents the extraction of the theoriticaly high efficiency of the frequency conversion [27].

In conclusion, we have designed and studied a new type of superconducting artificial atom with two internal DoF. The spectrum of this device is well described by considering two anharmonic oscillators coupled via nonlinear coupling terms. Coherent manipulation of the two DoF is demonstrated and the strong nonlinear coupling allows the observation of a coherent frequency conversion between the two internal DoF. If inserted in a microwave cavity this process should enable parametric amplification or generation of correlated microwave photons. Finally by reducing the critical current of the junctions, keeping the ratio L_J/L constant, one can increase the strength of the coupling term $g_{22}/2\pi$ up to 500 MHz providing a strong dispersive frequency shift proportional to the population of each mode. This should allow the realization of C-NOT quantum gate inside the two DoF of this artificial atom or enable an efficient readout of the camelback phase qubit state by probing the transition frequency of the a-mode. Considering the long list of unique and interesting features, this new artificial atom with two DoF and a V-shaped energy level structure is a valuable addition to the growing set of building blocks for superconducting quantum electronics.

We acknowledge C. Hoarau for his help on the electronic setup. We thank P. Milman and M. H. Devoret for fruitful discussions. We acknowledge the technical support of the PTA facility in CEA Grenoble and of the Nanofab facility in CNRS Grenoble. This work was supported by the European SOLID projects, by the French ANR "QUANTJO"and by the Nanoscience Foundation.

[1] D. Leibfried, et al, Rev. Mod. Phys., **75**, 281 (2003).
[2] F. Jelezko, et al, Phys. Rev. Lett. **92**, 076401 (2004).
[3] M. Fleischhauer, et al, Rev. Mod. Phys., **77**, 633 (2005).
[4] S. Y. Zhu, et al, Phys. Rev. Lett. **76**, 388 (1996).
[5] H. Xia, et al, Phys. Rev. Lett. **77**, 1032 (1996).
[6] Z. Y. Ou and L. Mandel, Phys. Rev. Lett. **61**, 50 (1988).
[7] A. Korotkov, Quantum Inf. Process. **8**, 51 (2009).
[8] J. Clarke, et al, Nature **453**, 1031 (2008).
[9] J. Claudon, et al., Phys. Rev. Lett. **93**, 187003 (2004).
[10] E. Lucero, et al, Phys. Rev. Lett. **100**, 247001 (2008).
[11] S. K. Dutta, et al., Phys. Rev. B **78**, 104510 (2008).
[12] L. S. Bishop, Nat. Phys. **5**, 105, (2008)
[13] R. Bianchetti, et al, Phys. Rev. Lett. **105**, 223601 (2010)
[14] J. Q. You and F. Nori, Nature **474**, 591, (2011)
[15] Y. Hu et al, Phys. Rev. A **84**, 012329 (2011)
[16] S. J. Srinivasan, et al., Phys. Rev. Lett. **106**, 083601 (2011)
[17] N. Bergeal, Nat. Phys. **6**, 296, (2010)
[18] K. Moon and S. M. Girvin, Phys. Rev. Lett. **95**, 140504 (2005)
[19] F. Marquardt, Phys. Rev. B **76**, 205416 (2007)
[20] E. Zakka-Bajjani, Nat. Phys. **7**, 599, (2011)
[21] D. Bouwmeester, A. K. Ekert, A. Zeilinger, The Physics of Quantum Information (Springer, 2000).
[22] E. Hoskinson, et al, Phys. Rev. Lett. **102**, 097004 (2009).
[23] The s- and a- modes are respectively the limit at zero current bias of the longitudinal and transverse mode defined in Ref.[27].
[24] V. Lefevre-Seguin, et al, Phys. Rev. B **46**, 5507 (1992).
[25] F. Balestro, et al, Phys. Rev. Lett. **91**, 158301 (2003).
[26] A. Fay, et al, Phys. Rev. B **83**, 184510 (2011).
[27] F. Lecocq, et al, Phys. Rev. Lett. **107**, 197002 (2011)
[28] F. Lecocq, et al, Nanotechnology **22** 315302 (2011).
[29] R. McDermott, et al, Science **307** 1299 (2005).
[30] M. Sillanpaa, et al, Nature **449** 438 (2007).
[31] J. M. Martinis, et al, Phys. Rev. Lett. **95**, 210503 (2005).
[32] With a rise time of 500ps this pulse fulfills the non-adiabatic condition with respect to the coupling strength g_{21} ($g_{21}^2/4 \approx 5$ GHz/ns$< V$ where $V \approx 7$ GHz/ns is the frequency change velocity in this experiment) but it is still adiabatic with respect to the plasma frequency of each mode.
[33] M. Steffen, et al, Phys. Rev. Lett. **97**, 050502 (2006).